Journal of Power Sources 246 (2014) 277–282

Contents lists available at ScienceDirect

Journal of Power Sources

journal homepage: www.elsevier.com/locate/jpowsour

Synthesis and hydrogen storage properties of Mg–10.6La–3.5Ni nanoparticles

Tong Liu [a,*], Yurong Cao [a], Chenggong Qin [a], Wusheng Chou [b], Xingguo Li [c,1]

[a] Key Laboratory of Aerospace Materials and Performance (Ministry of Education), School of Materials Science and Engineering, Beihang University, Beijing 100191, China
[b] School of Mechanical Engineering and Automation, Beihang University, Beijing 100191, China
[c] Beijing National Laboratory for Molecular Sciences (BNLMS), The State Key Laboratory of Rare Earth Materials Chemistry and Applications, College of Chemistry and Molecular Engineering, Peking University, Beijing 100871, China

HIGHLIGHTS

- We prepared Mg–10.6 wt. % La –3.5 wt. % Ni composite nanoparticles by HPMR method.
- The LaH_3 and Mg_2Ni nanoparticles disperse on the surface of Mg.
- Single crystalline Mg nanoparticles change into polycrystalline after activation.
- These nanoparticles show high hydrogen sorption kinetics and storage capacities.
- The hydrogen absorption activation energy of the nanoparticles is 39.1 kJ mol^{-1}.

GRAPHICAL ABSTRACT

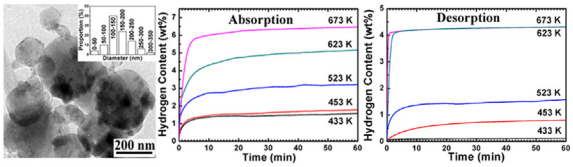

ARTICLE INFO

Article history:
Received 23 April 2013
Received in revised form
18 July 2013
Accepted 24 July 2013
Available online 2 August 2013

Keywords:
Hydrogen storage
Nanoparticles
Kinetics
Hydrogen plasma-metal reaction

ABSTRACT

The Mg–10.6 wt. % La–3.5 wt. % Ni nanoparticles are prepared by hydrogen plasma-metal reaction method. These nanoparticles are made of Mg, LaH_3 and a small amount of Mg_2Ni. The as-prepared Mg nanoparticles of 180 nm are single crystalline and quasi-spherical in shape, and they change into polycrystalline after activation. LaH_3 and Mg_2Ni nanoparticles are nearly spherical in shape with the mean particle size of 15 nm, and disperse on the surface of Mg. The Mg–10.6La–3.5Ni nanoparticles can absorb 3.2 wt. % H_2 in less than 15 min at 523 K and accomplish a high hydrogen storage capacity of 6.5 wt. % H_2 in less than 10 min at 673 K, almost reaching the theoretical gravimetric capacity. They can release 4.2 wt. % H_2 in 3 min at 623 K. The synergistic catalytic effect of LaH_3 and Mg_2Ni nanoparticles, the nanostructure and the low oxide content of Mg nanoparticles promote the hydrogen sorption process with the low hydrogen absorption activation energy of 39.1 kJ mol^{-1}.

1. Introduction

Hydrogen is considered as a promising energy carrier in future energy systems. However, due to the problems of low hydrogen storage capacity, unsafe and high cost, the conventional hydrogen storage methods through the compressed hydrogen gas and the cryogenic hydrogen liquid cannot meet the requirements of the

* Corresponding author. Tel.: +86 10 8231 6192; fax: +86 10 8231 4869.
E-mail addresses: tongliu@buaa.edu.cn (T. Liu), xgli@pku.edu.cn (X. Li).
[1] Tel.: +86 10 6275 3691; fax: +86 10 6276 5930.

0378-7753/$ – see front matter © 2013 Elsevier B.V. All rights reserved.
http://dx.doi.org/10.1016/j.jpowsour.2013.07.087

hydrogen applications, especially for the applications in the vehicles powered by fuel cells and in the hydrogen fueled internal combustion engines [1]. The key issue to realize the hydrogen economy is to develop a safe and efficient hydrogen storage approach [2]. Hydrogen storage via metal hydride materials has the advantages of high volumetric and gravimetric capacities and safety [1,3]. Many kinds of hydrogen storage materials, including $LaNi_5$ [4], Mg_2Ni [5], alanates [6], amides [7], carbon nanotubes [8] and metal-organic frameworks [9] have been developed up to now. Among these metal hydrides, MgH_2 is still considered to be one of the most attractive candidates due to its high theoretical gravimetric capacity of 7.6 wt. %, abundance and low cost. Nevertheless, the practical application of MgH_2 has not been fully achieved as the result of its slow hydrogen sorption kinetics and high thermodynamic stability [10]. In recent years, the addition of metal catalysts, such as Ni, Fe, V and Zn have been considered as one of the effective approaches to improve the hydrogen sorption kinetics of Mg hydrides [11–15]. By adding the catalyst of Fe, Puszkiel and co-workers [14] found that $Mg_{15}Fe$ can absorb 4.85 wt. % H_2 at 623 K in less than 10 min. Liang et al. [15] reported that the vanadium-catalyzed nanocrystalline magnesium hydride can release hydrogen completely under vacuum (0.015 MPa) within 200 s at 573 K and 900 s at 523 K, much faster than the mechanically milled MgH_2 which takes more than 2000 s to release 2 wt.% of hydrogen at 573 K. Among the compound catalysts, LaH_3 and Mg_2Ni are known as two of the most attractive candidates to decrease the stability of magnesium hydride [16,17]. Slattery reported that La_2Mg_{17} can absorb 3.1 wt. % H_2 at 623 K with the LaH_3 acting as a catalyst [16]. Liang and co-workers found that the Mg–$LaNi_5$ alloys catalyzed by Mg_2Ni and LaH_3 can absorb 4.1 wt. % H_2 within 1000 s at 423 K [17]. However, the average particle size of the Mg–$LaNi_5$ particles is rather big, about 60 μm. It is well known that the particle size greatly influences the hydrogen storage properties [10]. Yavari and co-workers reported that, with the FeF_3 of 5–10 nm as a catalyst, the MgH_2+2% FeF_3 can absorb 5.3 wt. % H_2 within 1000 s at 673 K [18]. Pelletier et al. also found that the MgH_2–Nb with Nb of 20 nm as a catalyst shows a low sorption activation energy of 65 ± 2 kJ mol^{-1} [19]. Therefore, to further improve the catalytic efficiency, it is necessary to produce Mg_2Ni and LaH_3 in nanosize.

Hydrogen plasma-metal reaction (HPMR) method is a novel vapor deposition processing and suitable for producing metallic nanoparticles industrially with high purity and low cost. Up to now, nanoparticles of several alloys and intermetallics have been fabricated by using HPMR approach, and the particle size can be tuned by controlling the hydrogen pressure and the current value [20–22]. In this work, we intend to fabricate the Mg–La–Ni nanoparticles using HPMR method and investigate the synergic effects of LaH_3 and Mg_2Ni nanoparticles on the hydrogen sorption properties and the phase transformations during the absorption and desorption cycle.

2. Experimental

The equipment for producing nanoparticles primarily contained an arc melting chamber and a collecting system, which was described elsewhere [20]. Firstly, Mg, La and Ni (purity > 99.9%) with a weight ratio of 49:15:36 were melted in the induction furnace. The $Mg_{49}La_{15}Ni_{36}$ ingot of 20 g was put in the reaction chamber. The Mg–La–Ni nanoparticles were produced by arc melting the ingot in a 50% Ar and 50% H_2 mixture of 0.1 MPa. The flow rate of the circulation gas for the collection of nanoparticles was 100 L min^{-1}. The arc current was selected as 80 A. Before the nanoparticles were taken out from the collection room, they were passivated with a mixture of argon and air.

The hydrogen absorption and desorption properties of the as-prepared Mg–La–Ni nanoparticles were evaluated using a Sieverts-type apparatus. The volume of the reactor chamber was about 60 ml, and the error of the measurement was less than 5%. After the Mg–La–Ni nanoparticles of 100 mg were put into the Sieverts reactor, the system was evacuated to 10^{-3} Pa. Then, the samples were heated up to 423, 453, 523, 623 and 673 K, respectively. A hydrogen pressure of 4 MPa was provided to make the Mg–La–Ni nanoparticles absorb hydrogen to measure the absorption kinetic curves. The desorption kinetic curves at various temperatures were measured at an initial pressure of about 100 Pa by evacuating the system.

The structural analyses of the Mg–La–Ni nanoparticles before and after the hydrogen sorption were carried out by X-ray diffraction (XRD) using a Rigaku X-ray diffractometer with monochromatic Cu Kα radiation. The morphology, size distribution and shape of the nanoparticle samples before and after the hydrogen sorption were observed by TEM using JEOL-JSM-2100 at an accelerating voltage of 200 kV. The energy dispersive X-ray spectroscopy (EDX) was used to determine the contents of Mg, La and Ni in the Mg–La–Ni nanoparticles.

3. Results and discussion

3.1. Particle features

Fig. 1 displays the TEM image of the as-prepared Mg–La–Ni nanoparticles. It is apparently observed that there are two kinds of particles. The big particles vary from 100 to 350 nm with an average size of about 180 nm. The fine particles of about 15 nm in nearly spherical shape are dispersed on the surface of each big particle. It is interesting to find that the big particles are quasi-spherical in shape, which is different from the pure Mg ultrafine particles prepared by HPMR [23]. We suggest that in the present study, the addition of La and Ni promotes the homogeneous growth of Mg particles. Fig. 2 shows the high resolution TEM images of the Mg–La–Ni nanoparticles. It is observed that the small particle belongs to a polycrystalline structure. One lattice spacing is evaluated to be 0.326 nm in Fig. 2(a) for the small particle, which corresponds to the (111) plane of LaH_3. It can be seen from Fig. 2(b) that the measured lattice spacing of the big particle is 0.246 nm, which

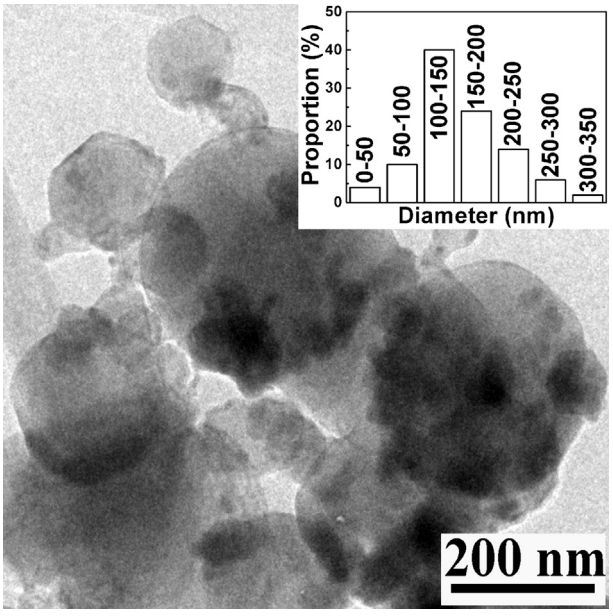

Fig. 1. TEM image of the as-prepared Mg–La–Ni nanoparticles.

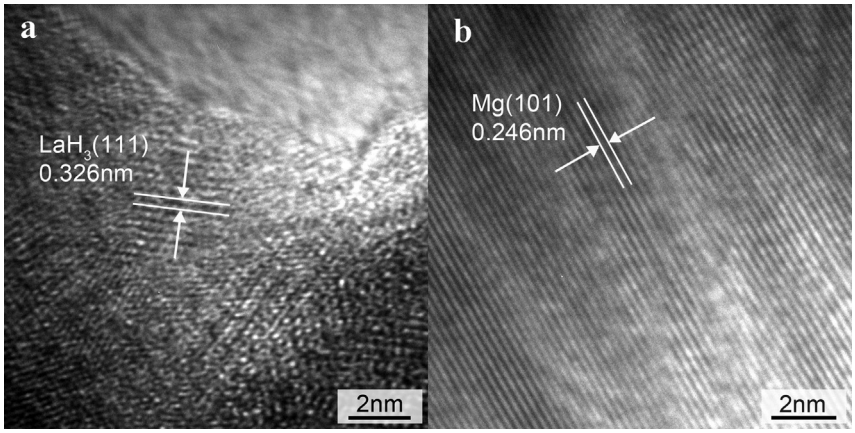

Fig. 2. HR-TEM images of the Mg–La–Ni nanoparticles: (a) the small particle on the matrix. (b) The matrix of Mg–La–Ni nanoparticle.

corresponds to the hcp-Mg (101) plane. This indicates that the big particle is Mg with a single crystal structure. The crystal structure of the Mg–La–Ni nanoparticles is also supported by the XRD results discussed hereafter. The EDX result in Fig. 3 displays that the average contents of La and Ni in the Mg–La–Ni nanoparticles are 10.6 wt. % and 3.5 wt. %, respectively. Hereafter, the Mg–La–Ni sample is referred as the Mg–10.6La–3.5Ni nanoparticles. The lower contents of La and Ni in the as-prepared nanoparticle than in the master ingot are due to the higher evaporation rate of Mg than those of La and Ni during the HPMR process.

Fig. 4 shows the XRD patterns of the as-prepared Mg–10.6La–3.5Ni nanoparticles and the samples obtained after the hydrogen absorption and desorption at 673 K. Several hydrides and intermetallic compounds such as TiAl [20], CoAl [22] and TiH_2 [23] have been prepared directly using the HPMR method. It is found in Fig. 4(a) that the as-prepared Mg–10.6La–3.5Ni nanoparticles are composed of α-Mg (hcp) dominantly, and some LaH_3 and a little amount of Mg_2Ni. The lattice constants of Mg calculated from the XRD data are $a = 3.209$ Å and $c = 5.208$ Å, similar with the standard data of α-Mg (PDF35-0821, $a = 3.209$ Å, $c = 5.211$ Å), indicating that no La and Ni atoms dissolve in Mg. This agrees with the fact that according to the Mg–La and Mg–Ni binary diagrams, La and Ni are almost immiscible with Mg and no Mg–La/Ni solid solution can be formed at room temperature [23]. The metallic nanoparticles often become more pyrophoric than the corresponding coarse particles. It is worth to note that the diffraction peak of MgO around 42.9°, which often appears in the Mg particles prepared by HPMR [22], cannot be detected in the present XRD pattern. This reveals that the addition of La and Ni effectively suppresses the oxidation tendency of Mg, leading to the decrease of MgO content in the Mg–10.6La–3.5Ni nanoparticles. From the XRD pattern in Fig. 4(b), it can be found that during the hydrogen absorption process at 673 K, the Mg–10.6La–3.5Ni nanoparticles transform into MgH_2, LaH_3 and Mg_2NiH_4 phase. It is observed from Fig. 4(c) that during the hydrogen desorption at 673 K, MgH_2 decomposes into Mg completely and Mg_2Ni recovers from Mg_2NiH_4. On the other hand, the decomposition of LaH_3 does not happen, which agrees with the previous studies that LaH_3 will not release hydrogen at this temperature [24,25]. It is proposed that these LaH_3 nanoparticles are crucial to catalyze the hydrogenation of Mg.

Fig. 5(a) shows the TEM image of the Mg–10.6La–3.5Ni nanoparticles after the dehydrogenation. It is interesting to find that after the hydrogen desorption, the Mg nanoparticles are still quasi-spherical shape with an average size of about 180 nm, but they change from single crystal to polycrystalline. The mechanism for the transformation of Mg nanoparticle from single crystalline to polycrystalline can be concluded as follows. The mechanism for this transformation can be explained as follows. During the hydrogen absorption process, Mg of single crystalline changed into MgH_2 at the expense of volume expansion. Then, MgH_2 decomposes into Mg during the hydrogen desorption, accompanied by a volume decrease. The volume increase and cause cracks in the particle and

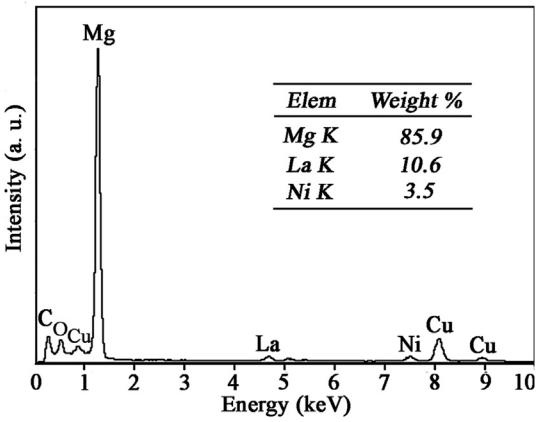

Fig. 3. The energy dispersive X-ray spectroscopy obtained from the Mg–10.6La–3.5Ni nanoparticles.

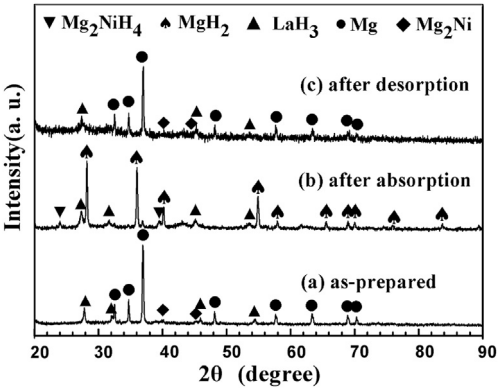

Fig. 4. XRD patterns of the Mg–10.6La–3.5Ni nanoparticles: (a)as-prepared, (b) after the absorption under 4 MPa hydrogen pressure at 673 K, and (c) after the hydrogen desorption under 100 Pa at 673 K.

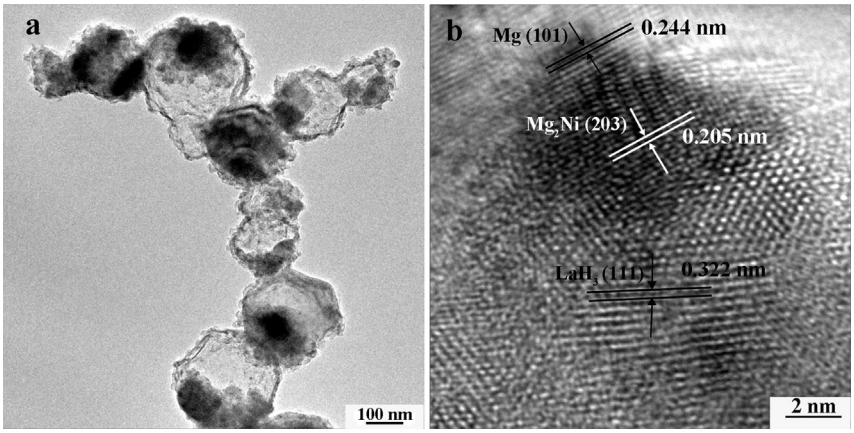

Fig. 5. TEM image of the Mg–10.6La–3.5Ni nanoparticles after the dehydrogenation (a) and HR-TEM image of one Mg–10.6La–3.5Ni nanoparticle after the dehydrogenation (b).

the grain boundary will be produced. Therefore, Mg nanoparticles change from single crystalline into polycrystalline. It is also discernable from Fig. 5(a) that the fine black dots known as LaH_3 and Mg_2Ni nanoparticles of about 15 nm are distributed on the surface of Mg. Fig. 5(b) shows the HR-TEM image of one typical Mg–10.6La–3.5Ni nanoparticle after the dehydrogenation. The lattice fringes are clearly seen in the big particle and the measured lattice spacing is 0.244 nm, which corresponds to the Mg (101) plane. The lattice spacings of the small particles are evaluated to be 0.322 nm and 0.205 nm, which correspond to the (111) plane of LaH_3 and (203) plane of Mg_2Ni, respectively.

On the basis of the analysis above, the formation of the Mg–10.6La–3.5Ni nanoparticles by HPMR and their phase transformations during the hydrogen absorption and desorption processes can be summarized by the following equations.

$$Mg + La + Ni + H_2 \rightarrow Mg + LaH_3 + Mg_2Ni \ \text{(HPMR process)} \quad (1)$$

$$Mg + LaH_3 + Mg_2Ni + H_2 \rightarrow MgH_2 + LaH_3 + Mg_2NiH_4 \ \text{(Absorption)} \quad (2)$$

$$MgH_2 + LaH_3 + Mg_2NiH_4 \rightarrow Mg + LaH_3 + Mg_2Ni + H_2 \ \text{(Desorption)} \quad (3)$$

3.2. Hydrogen storage properties

The activation treatment through annealing at 673 K in vacuum and in hydrogen for several cycles is often required for the micro-size Mg particles. Even after this activation process, Mg in microsize could absorb only 1.5 wt. % H_2 within 2 h at a temperature as high as 673 K [10]. Fig. 6(a) shows the hydrogen absorption curve of the Mg–10.6La–3.5Ni nanoparticles at different temperatures. It can be observed that the hydrogen absorption content enlarges remarkably with time in the initial absorption stage and the hydrogen absorption rate also increases with increasing the temperature from 433 to 673 K. They can absorb hydrogen even at 523 K and reach a value of 3.2 wt. % in less than 15 min, quite faster than the micro-sized and some catalyzed Mg particles [2,11,13,26,27]. Moreover, it is worth of noting that they can absorb 6.5 wt. % H_2 at 673 K, almost reaching the theoretical gravimetric capacity of the Mg–10.6La–3.5Ni nanoparticles. The hydrogen storage capacities at 433, 453 and 623 K are 1.6, 1.8 and 4.0 wt. %, respectively. Wu et al. [28] reported that the ball-milled Mg–10Ni–2Mm alloy reached a maximum hydrogen storage capacity of about 3.2 wt. % in 2 h at 573 K. Ouyang et al. [29] observed that $Mg_3LaNi_{0.1}$ alloy can absorb 2.73 wt. % hydrogen at 530 K. It is clear that the hydrogen storage capacity of the Mg–10.6La–3.5Ni nanoparticles at 523 K was higher than those of the Mg–10Ni–2Mm and $Mg_3LaNi_{0.1}$ alloys at 530 K and 573 K. Pan et al. [30] observed that the hydrogen storage capacity of the Mg particles catalyzed by the micro-sized LaH3 and Mg2Ni did not reach 2 wt. % within 7500 s at 573 K. It is obvious that the hydrogen storage properties of the Mg–10.6La–3.5Ni nanoparticles are better than the micro-sized Mg–LaH_3–Mg_2Ni. Fig. 6(b) shows the hydrogen desorption curve of the Mg–10.6La–3.5Ni nanoparticles at different temperatures. It can be seen that at 673 K, the hydrogen desorption content enlarges remarkably with the increase of the temperature in the initial desorption stage and reaches a value of 4.2 wt. % in 3 min. At 523 K, the Mg–10.6La–3.5Ni nanoparticles can dehydrogenate nearly 2.9 wt. % H_2, displaying the improved sorption kinetics. It is clear that the Mg–10.6La–3.5Ni nanoparticles show superior hydrogen sorption rate and storage capacity to both the ball-milled Mg–10Ni–2Mm and Mg_3La alloys. Zhu et al. [31] reported that the MgH_2-10 wt.% LaH_3 composite can only desorb 0.22 wt. % H_2 in 28 min at 573 K. Dong [32] and co-workers found that the Mg_3La alloy catalyzed by LaH_3 can release 2.77 wt. % H_2 at 573 K. Liang [33] and co-workers reported that the hydrogenation absorption capacity of Mg–Mg_2Ni composites were less than 2 wt. % in 1 h at 573 K. Compared with these results, it is clear that the catalytic effect of the synergy of LaH_3 and Mg_2Ni nanoparticles is better than that of LaH_3 or Mg_2Ni alone.

The activation energy for hydrogen absorption is usually calculated from the JMAK (Johnson–Mehl–Avrami–Kolmogorov) model and the Arrhenius theory. On the basis of JMAK model, the hydrogen absorption kinetics can be expressed in the following linear equation:

$$\ln[-\ln(1-\alpha)] = \eta \ln k + \eta \ln t \quad (4)$$

where α is the fraction transformed at time t, k is an effective kinetic parameter, η is the Avrami exponent of reaction order. For the experimental data of 453, 523 and 673 K, by plotting $\ln[-\ln(1-\alpha)]$ vs. $\ln(t)$ shown in Fig. 7, each temperature provided a straight line with a slope η and an intercept $\eta \ln(k)$. After calculating the rate constant k from the η value, the apparent activation energy for the absorption process was evaluated from the Arrhenius equation:

$$K = A \cdot \exp\left(E_a / RT\right) \quad (5)$$

where A is a temperature-independent coefficient, E_a is the apparent activation energy, R is the gas constant (8.314 J mol^{-1} K^{-1}), and T is

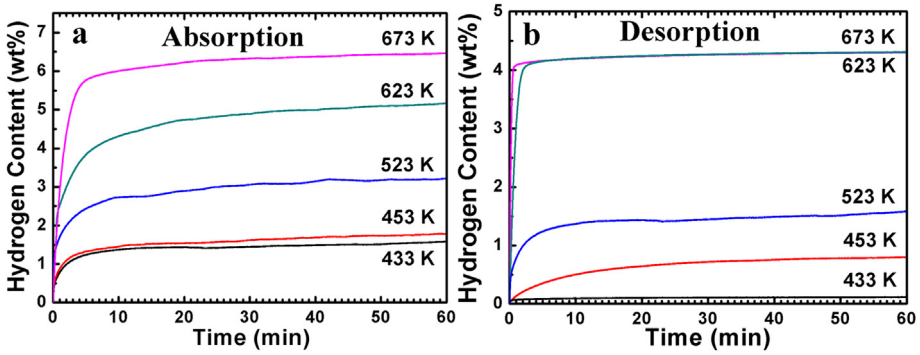

Fig. 6. Hydrogen absorption curves of the Mg–10.6La–3.5Ni nanoparticles at 433, 453, 523, 623 and 673 K under 4 MPa hydrogen pressure (a) and the desorption curves at 433, 453, 523, 623 and 673 K (b).

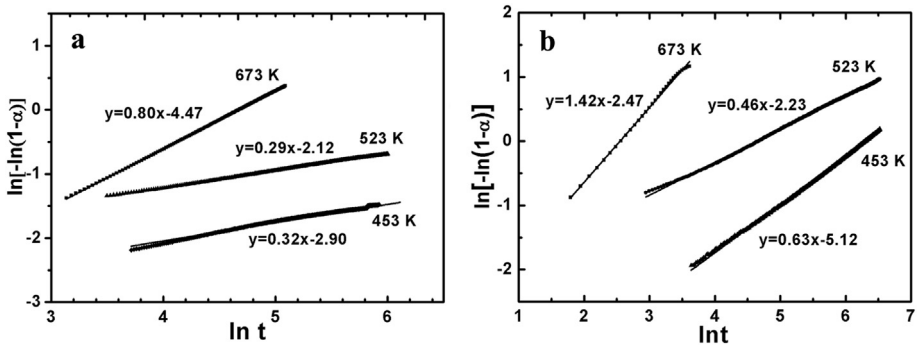

Fig. 7. Plots $\ln(-\ln(1-\alpha))$ vs. $\ln(t)$ for the hydrogen absorption (a) and desorption (b) of the Mg–10.6La–3.5Ni nanoparticles.

the absolute temperature. The absorption and desorption plots of $\ln(k)$ vs. $1000/T^{-1}$ are shown in Fig. 8. It is found that the fits (R^2) of these two plots are 0.928 and 0.978, respectively, implying that the experimental data can be evaluated by JMAK model and Arrhenius theory. The calculated hydrogen absorption activation energy of the Mg–10.6La–3.5Ni nanoparticles is 39.1 kJ mol^{-1}, quite lower than that of the micro-size Mg particles (95–130 kJ mol^{-1}) [34]. It is also lower than that of the magnesium thin film (72 kJ mol^{-1}) and the Mg ultrafine particles of 38 nm (115 kJ mol^{-1}) [35,36]. The desorption activation energy of the Mg–10.6La–3.5Ni nanoparticles is 77.6 kJ mol^{-1}, which is also lower than that of the Mg particles of 38 nm, 126 kJ mol^{-1} [36].

It is well known that the hydrogenation rate of Mg is affected by several factors.

Firstly, the surface of pure magnesium without catalytic additives requires a very high energy for the dissociation of H_2. In the present work, the LaH_3 and Mg_2Ni nanoparticles disperse on the surface of Mg particles act as catalysts to decrease the dissociation energy of H_2 and improve the hydrogen sorption kinetics of Mg. It was reported that Mg_2Ni has a catalytic effect on both hydriding and dehydriding processes by easing the dissociation and recombination of hydrogen due to the partially filled 3d electron orbits of Ni [37]. Secondly, the formation rate of MgH_2 on the Mg surface and along the grain boundaries are the critical factors to impact the hydrogenation capacity and kinetics, because the diffusion coefficient of H in MgH_2 is much smaller than that in Mg [38]. It was also reported that the hydrogenation rate of the magnesium decreased with increasing the hydride layer thickness [39]. In this work, the fine particle size decreases the thickness of MgH_2, and the nano-sized grain of Mg accelerates the H diffusion, resulting in the improved hydrogen sorption kinetics of Mg particles. Additionally, it is known that the oxide layer of Mg particles prevents hydrogen

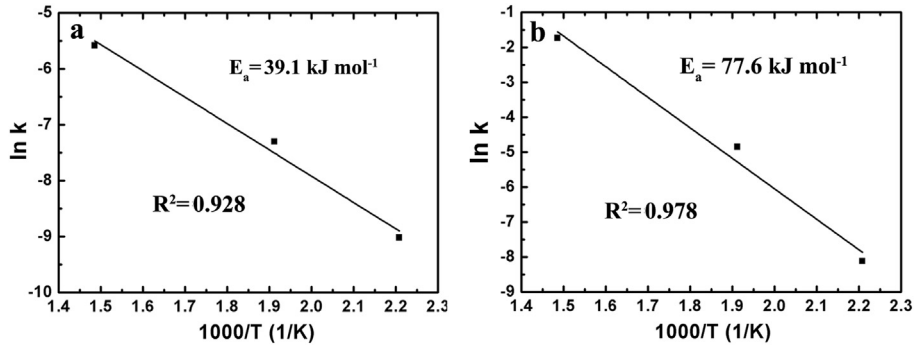

Fig. 8. Absorption plot (a) and desorption plot (b) of ln k vs. $1000/T^{-1}$ of the Mg–10.6La–3.5Ni nanoparticles.

from transporting into Mg. In this work, the decrease of oxide content due to the dispersion of LaH_3 and Mg_2Ni on the surface of Mg particles accelerates the sorption of H on the surface of Mg particles. Thus, the high hydrogen sorption rate and storage capacity with a very low hydrogen absorption activation energy are attributed to the synergistic catalytic effect of LaH_3 and Mg_2Ni nanoparticles, the decreased oxide content and the fine particle/grain size. The Mg–10.6La–3.5Ni nanoparticles with high sorption kinetics, high storage capacity, and low hydrogenation temperature, are a promising candidate for hydrogen storage.

4. Conclusions

Mg–10.6 wt. % La–3.5 wt. % Ni nanoparticles were prepared from the $Mg_{49}La_{15}Ni_{36}$ ingot by HPMR method. These nanoparticles were made of Mg, LaH_3 and a little amount of Mg_2Ni. Mg nanoparticles of single crystalline were quasi-spherical in shape, varying from 100 to 350 nm with an average size of about 180 nm. The LaH_3 and Mg_2Ni nanoparticles of 15 nm dispersed on the surface of Mg nanoparticles. After one sorption cycle for the activation, Mg nanoparticles changed into polycrystalline. The addition of La and Ni played a crucial role in enhancing the sorption kinetics properties of the Mg–10.6La–3.5Ni nanoparticles. These nanoparticles can absorb hydrogen at 523 K and reach a value of 3.2 wt. % in less than 15 min. Moreover, they can absorb 6.5 wt. % H_2 in less than 10 min at 673 K. It can also release 4.2 wt. % H_2 in 3 min at 623 K. The synergistic catalytic effect of LaH_3 and Mg_2Ni nanoparticles, nanostructure and low oxide content of Mg nanoparticles promoted the hydrogen sorption process with low hydrogen absorption and desorption activation energies.

Acknowledgments

The authors acknowledge the support of this work by MOST of China (No. 2011AA03A408 and No. 2013CB035503), the Aeronautical Science Foundation of China (No. 2011ZF51065), and the Scientific Research Foundation for the Returned Overseas Chinese Scholars, State Education Ministry. We also thank Professor Huiping Duan and Center for Instrumental Analysis and Research, Beihang University for the technical aid in TEM observation.

References

[1] B. Sakintuna, F. Lamari-Darkrim, M. Hirscher, Int. J. Hydrogen Energy 32 (2007) 1121–1140.
[2] H.Y. Shao, G.B. Xin, J. Zheng, X.G. Li, E. Akibaa, Nano Energy 1 (2012) 590–601.
[3] T. Liu, C.G. Qin, M. Zhu, Y.R. Cao, H.L. Shen, X.G. Li, J. Power Sources 219 (2012) 100–105.
[4] A. Demircan, M. Demiralp, Y. Kaplan, M.D. Mat, T.N. Veziroglu, Int. J. Hydrogen Energy 30 (2005) 1437–1446.
[5] T. Liu, H.L. Shen, Y. Liu, L. Xie, J.L. Qu, H.Y. Shao, X.G. Li, J. Power Sources 227 (2013) 86–93.
[6] S.I. Orimo, Y. Nakamori, J.R. Eliseo, A. Züttel, C.M. Jensen, Chem. Rev. 107 (2007) 4111–4132.
[7] H.Y. Leng, T. Ichikawa, S. Hino, N. Hanada, S. Isobe, H. Fujii, J. Power Sources 156 (2006) 166–170.
[8] Y.L. Kuan, T.T. Wen, J.Y. Tsong, J. Power Sources 196 (2011) 3389–3394.
[9] J.L.C. Rowsell, O.M. Yaghi, Angew. Chem. Int. Ed. 44 (2005) 4670–4679.
[10] A. Zaluska, L. Zaluski, J.O. StromeOlsen, J. Alloys Compd. 288 (1999) 217–225.
[11] R.L. Holtz, M.A. Imam, J. Mater. Sci. 34 (1999) 2655–2663.
[12] T. Liu, T.W. Zhang, C.G. Qin, M. Zhu, X.G. Li, J. Power Sources 196 (2011) 9599–9604.
[13] T. Liu, T.W. Zhang, X.Z. Zhang, X.G. Li, Int. J. Hydrogen Energy 36 (2011) 3515–3520.
[14] J.A. Puszkiel, P.A. Larochette, F.C. Gennari, J. Power Sources 186 (2009) 185–193.
[15] G. Liang, J. Huot, S. Boily, A.V. Neste, R. Schulz, J. Alloys Compd. 291 (1999) 295–299.
[16] D.K. Slattery, Int. J. Hydrogen Energy 20 (1995) 971–973.
[17] G. Liang, J. Huot, S. Boily, N.A. Van, R. Schulz, J. Alloys Compd. 297 (2000) 261–265.
[18] A.R. Yavari, A. LeMoulec, F.R. de Castro, S. Deledda, O. Friedrichs, W.J. Botta, G. Vaughan, T. Klassen, A. Fernandez, A. Kvick, Scr. Mater. 52 (2005) 719–724.
[19] J.F. Pelletier, J. Huot, M. Sutton, R. Schulz, A.R. Sandy, L.B. Lurio, S.G.J. Mochrie, Phys. Rev. B 63 (2001) 052103.
[20] T. Liu, T.W. Zhang, M. Zhu, C.G. Qin, J. Nanopart. Res. 14 (2012) 73833.
[21] T. Liu, C.G. Qin, T.W. Zhang, Y.R. Cao, M. Zhu, X.G. Li, J. Mater. Chem. 22 (2012) 19831.
[22] T. Liu, M. Zhu, H.L. Shen, C.G. Qin, Y.R. Cao, J. Nanopart. Res. 15 (2013) 1476.
[23] T. Liu, Y.H. Zhang, X.G. Li, Scr. Mater. 48 (2003) 397–402.
[24] A. Zaluska, L. Zaluski, J.O. Strom-Olsen, Appl. Phys. A 72 (2001) 157–165.
[25] C.X. Shang, M. Bououdina, Z.X. Guo, Mater. Trans. 44 (2003) 2356–2362.
[26] M.Y. Song, J.L. Bobet, B. Darriet, J. Alloys Compd. 340 (2002) 256–262.
[27] T.R. Jensen, A. Andreasen, T. Vegge, J.W. Andreasen, K. Ståhl, A.S. Pedersen, Int. J. Hydrogen Energy 31 (2006) 2052–2062.
[28] Y. Wu, W. Han, S.X. Zhou, M.V. Lototsky, J.K. Solberg, V.A. Yartys, J. Alloys Compd. 466 (2008) 176–181.
[29] L.Z. Ouyang, F.X. Qin, M. Zhu, Scr. Mater. 55 (2006) 1075–1078.
[30] Y.B. Pan, Y.F. Wu, Q. Li, Int. J. Hydrogen Energy 36 (2011) 12892–12901.
[31] X.L. Zhu, L.C. Pei, Z.Y. Zhao, B.Z. Liu, S.M. Han, R.B. Wang, J. Alloys Compd. 577 (2013) 64–69.
[32] H.W. Dong, L.Z. Ouyang, T. Sun, M. Zhu, J. Rare Earths 26 (2008) 303–306.
[33] G. Liang, S. Boily, J. Huot, A.V. Neste, R. Schulz, J. Alloys Compd. 267 (1998) 302–306.
[34] J.F. Fernandez, C.R. Sanchez, J. Alloys Compd. 340 (2002) 189–198.
[35] M. Johansson, C.W. Ostenfeld, I. Chorkendorff, Phys. Rev. B 74 (2006) 193408.
[36] N.S. Norberg, T.S. Arthur, S.J. Fredrick, A.L. Prieto, J. Am. Chem. Soc. 133 (2011) 10679–10681.
[37] H. Gu, Y.F. Zhu, L.Q. Li, Int. J. Hydrogen Energy 34 (2009) 1405–1410.
[38] D.S. Sholl, J. Alloys Compd. 446 (2007) 462–468.
[39] X. Yao, Z.H. Zhu, H.M. Cheng, G.Q. Lu, J. Mater. Res. 23 (2008) 336–340.